



1     **Exploring the drivers of the elevated ozone production in Beijing in**  
2                                   **summertime during 2005-2016**

3     Wenjie Wang<sup>1</sup>, David D. Parrish<sup>2</sup>, Xin Li<sup>1,3,4,\*</sup>, Min Shao<sup>2,1</sup>, Ying Liu<sup>1</sup>, Sihua Lu<sup>1</sup>, Min  
4     Hu<sup>1</sup>, Yusheng Wu<sup>1,#</sup>, Limin Zeng<sup>1</sup>, Yuanhang Zhang<sup>1</sup>

5

6

7             <sup>1</sup> State Key Joint Laboratory of Environmental Simulation and Pollution Control,  
8     College of Environmental Sciences and Engineering, Peking University, Beijing,  
9     China

10            <sup>2</sup> Institute for Environmental and Climate Research, Jinan University,  
11     Guangzhou 511443, China

12            <sup>3</sup> International Joint Laboratory for Regional Pollution Control, Ministry of  
13     Education, Beijing, 100816, China

14            <sup>4</sup> Collaborative Innovation Centre of Atmospheric Environment and Equipment  
15     Technology, Nanjing University of Information Science & Technology, Nanjing,  
16     210044, China

17            # now at Department of Physics, University of Helsinki, Helsinki, Finland

18

19

20

21

22            \* Corresponding author.

23            Address: College of Environmental Sciences and Engineering, Peking  
24     University, Beijing 100871, China

25            Phone: 86-10-62757973

26            Email: [li\\_xin@pku.edu.cn](mailto:li_xin@pku.edu.cn)

27



## 28 **Abstract**

29 In the past decade, average  $PM_{2.5}$  concentrations decreased rapidly under the  
30 strong pollution control measures in major cities in China; however, ozone ( $O_3$ )  
31 pollution emerged as a significant problem. Here we examine a unique (for China) 12-  
32 year data set of ground-level  $O_3$  and precursor concentrations collected at an urban site  
33 in Beijing (PKUERS), where the maximum daily 8 h average (MDA8)  $O_3$  concentration  
34 and daytime  $O_x$  ( $O_3 + NO_2$ ) concentration in August increased by  $2.3 \pm 1.2$  ppbv ( $+3.3$   
35  $\pm 1.8\%$ )  $yr^{-1}$  and  $1.4 \pm 0.6$  ( $+1.9 \pm 0.8\%$ )  $yr^{-1}$  respectively from 2006 to 2016. In contrast,  
36 daytime concentrations of nitrogen oxides ( $NO_x$ ) and the OH reactivity of volatile  
37 organic compounds (VOCs) both decreased significantly. Over this same time, the  
38 decrease of particulate matter, and thus the aerosol optical depth, led to enhanced solar  
39 radiation and photolysis frequencies, with near-surface  $j(NO_2)$  increasing at a rate of  
40  $3.6 \pm 0.8\%$   $yr^{-1}$ . We use an observation based box model to analyze the combined effect  
41 of solar radiation and ozone precursor changes on ozone production rate,  $P(O_3)$ . The  
42 results indicate that the ratio of the rates of decrease of VOCs and  $NO_x$  (about 1.1) is  
43 inefficient in reducing ozone production in Beijing.  $P(O_3)$  increased during the decade  
44 due to more rapid atmospheric oxidation caused to a large extent by the decrease of  
45 particulate matter. This elevated ozone production was driven primarily by increased  
46 actinic flux due to  $PM_{2.5}$  decrease and to a lesser extent by reduced heterogeneous  
47 uptake of  $HO_2$ . Therefore, the influence of  $PM_{2.5}$  on actinic flux and thus on the rate of  
48 oxidation of VOCs and  $NO_x$  to ozone and to secondary aerosol (i.e., the major  
49 contributor to  $PM_{2.5}$ ) is important for determining the atmospheric effects of controlling  
50 the emissions of the common precursors of  $PM_{2.5}$  and ozone when attempting to control  
51 these two important air pollutants.

52

53

54



## 55 **1 Introduction**

56 Tropospheric ozone (O<sub>3</sub>) plays a key role in the oxidizing capacity of the  
57 atmosphere and affects the global climate; high concentrations of ground-level ozone  
58 are harmful to human health and ecosystems (Monks et al., 2015; Fiore et al., 2009).  
59 Ozone is produced rapidly in polluted air by photochemical oxidation of volatile  
60 organic compounds (VOCs) in the presence of nitrogen oxides (NO<sub>x</sub> ≡ NO + NO<sub>2</sub>)  
61 (Atkinson, 2000). In recent years, China has undergone rapid economic development,  
62 resulting in higher demand for energy, and greater usage of fossil fuels. As a result,  
63 high emissions to the atmosphere produce heavy pollution in eastern China, which  
64 now suffers from severe ozone pollution, especially in urban areas, where the daily  
65 maximum 8 h average (MDA8) ozone level often exceeds the standard of 80 ppb  
66 (Jinfeng et al., 2014; Wang et al., 2011; Zhang et al., 2014; Lu et al., 2018; Li et al.,  
67 2019). A recent study reported that the national warm-season (April–September)  
68 fourth highest MDA8 ozone level (86.0 ppb) and the number of days with MDA8  
69 values of > 70 ppb was much higher than regional averages in Japan, South Korea,  
70 Europe, or the United States (Lu et al., 2018). Satellite observations found that  
71 regional ozone concentrations in eastern China increased by 7% between 2005 and  
72 2010 (Verstraeten et al., 2015). From 2013 to 2017, the O<sub>3</sub> concentrations in 74 cities  
73 as a whole showed an upward trend with Beijing–Tianjin–Hebei region being the most  
74 serious (Li et al., 2019; Lu et al., 2018). Better understanding of the causes of elevated  
75 ozone in China is important for developing effective emission control strategies to  
76 reduce the ozone pollution problem.

77 Aerosols impact ozone production primarily in two ways: alteration of photolysis  
78 rates by aerosol radiative influence and heterogeneous reactions occurring on the  
79 aerosol surface. The reduction of photolysis frequencies by the extinction effect of  
80 aerosol and thus its influence on ozone production has been explored in the past  
81 (Dickerson et al., 1997; Castro et al., 2001; Real and Sartelet, 2011; Gerasopoulos et al.,  
82 2012; Wang et al., 2019). Absorbing aerosols reduce photolysis frequencies



83 throughout the boundary layer, and as a result decrease near-surface photochemical  
84 ozone production (de Miranda et al., 2005; Jacobson, 1998; Wendisch et al., 1996; Raga  
85 et al., 2001). Conversely, scattering aerosols in the boundary layer increase photolysis  
86 frequencies throughout the troposphere, and thereby increase ozone production aloft  
87 (Jacobson, 1998; Tian et al., 2019; Dickerson et al., 1997). The importance of aerosol  
88 heterogeneous reactions in ozone photochemistry in China has been previously  
89 investigated in model studies (Lou et al., 2014; Li et al., 2018; Xu et al., 2012; Li et al.,  
90 2019). The effects of NO<sub>2</sub>, NO<sub>3</sub>, and N<sub>2</sub>O<sub>5</sub> heterogeneous reactions showed opposite  
91 O<sub>3</sub> concentration changes in VOC-limited and NO<sub>x</sub>-limited regions. In a VOC-limited  
92 region, NO<sub>2</sub>, NO<sub>3</sub>, and N<sub>2</sub>O<sub>5</sub> heterogeneous reactions lead to ozone concentration  
93 increases (Lou et al., 2014; Xu et al., 2012). The heterogeneous reaction of HO<sub>2</sub>  
94 decreases ozone production in both VOC-limited and NO<sub>x</sub>-limited regions by  
95 decreasing the reaction rate of HO<sub>2</sub> with NO (Lou et al., 2014; Li et al., 2019).

96 In the past decade, Eastern China has experienced severe fine particulate matter  
97 (PM<sub>2.5</sub>) pollution in winter (Zhang et al., 2016), and this issue has been the main focus  
98 of the government's air pollution control strategy. These stringent emission control  
99 measures have significantly decreased the concentrations of particulate matter in many  
100 Chinese cities. During 2008-2013, ground-level PM<sub>2.5</sub> estimated from satellite-  
101 retrieved aerosol optical depth (AOD) in China declined at a rate of 0.46 μg m<sup>-3</sup> year<sup>-1</sup>  
102 (Ma et al., 2016b). Another study indicated that the annual average concentration of  
103 PM<sub>2.5</sub> in Beijing decreased by 1.5 μg m<sup>-3</sup> year<sup>-1</sup> and 27% in total from 2000 to 2015  
104 under the implementation of 16 phases' air pollution control measures (Lang et al.,  
105 2017). Hu et al (2017) reported that PM<sub>2.5</sub> in Beijing declined significantly from 2006  
106 to 2016, and meanwhile solar radiation increased (Hu et al., 2017). However, despite  
107 the reduction in emissions of particulate matter (PM) and ozone precursors, ozone  
108 concentrations increased, even while PM concentrations decreased.

109 In Beijing, the second largest city in China, with rapid economic development and  
110 urbanization in recent years, ozone pollution is one of the worst among China's cities.  
111 Thus, Beijing is a representative city in which to study urban ozone pollution in China.



112 Despite extensive study of the relationship between ozone and its precursors in Beijing  
113 and other mega cities in China (Zhang et al., 2014;Chou et al., 2011;Lu et al., 2019;Liu  
114 et al., 2012), there remains a lack of understanding of the cause of the long-term ozone  
115 increase that accompanies reductions in precursor emissions. In this study, we utilize  
116 measurements from a representative urban site in Beijing to explore how the variations  
117 in solar radiation and heterogeneous reactions influence the trend of ozone and the  
118 coupling effect of aerosol and ozone precursor changes on ozone production. Our  
119 overall goal is to determine the extent to which increasing actinic flux caused by the  
120 decline in PM contributed to the observed increase in ozone concentrations. This  
121 research provides a clearer understanding of how efforts to reduce PM concentrations  
122 affect ozone concentrations, and thus informs air quality improvement efforts in  
123 China's urban areas.

## 124 **2 Materials and methods**

### 125 **2.1 Measurements of air pollutants, photolysis frequencies and aerosol surface** 126 **concentration**

127 Ambient air pollutants and photolysis frequencies were measured at an urban site  
128 in Beijing in August between 2005 and 2016. The site (39.99° N, 116.31°E) was located  
129 on the roof of a six story building (~20m above the ground level) on the campus of  
130 Peking University (PKUERS) near the 4th Ring Road with high density of traffic, but  
131 without obvious industrial or agricultural sources (Wehner et al., 2008). Temporal  
132 trends of air pollutants and composition of VOCs are thought to be representative for  
133 the whole of Beijing (Wang et al., 2010;Xu et al., 2011;Zhang et al., 2012). Measured  
134 parameters include O<sub>3</sub>, NO<sub>x</sub>, CO, SO<sub>2</sub>, C<sub>2</sub> - C<sub>10</sub> VOCs, photolysis frequencies and  
135 aerosol surface concentration. The measurement techniques are included in the Table 1.

136 During 2006 and 2008, ambient levels of VOCs were measured using an online  
137 GC-FID system built by the Research Center for Environmental Changes (RCEC;  
138 Taiwan). A detailed description of this system and QA/QC procedures can be found in



139 Wang et al. (Wang et al., 2004). During August 2007 and 2009, ambient VOCs were  
140 measured using a commercial GC-FID/PID system (Syntech Spectra GC955 series  
141 600/800 analyzer) (Xie et al., 2008; Zhang et al., 2014). From 2010 to 2016, VOCs were  
142 measured using a cryogen-free online GC-MS/FID system developed by Peking  
143 University. A detailed description of this system and QA/QC procedures can be found  
144 in Yuan et al. and Wang et al. (Yuan et al., 2012; Wang et al., 2014). Formaldehyde  
145 (HCHO) concentrations were measured by a Hantzsch fluorimetry.

146 Photolysis frequencies (including  $j(\text{O}^1\text{D})$ ,  $j(\text{NO}_2)$ ,  $j(\text{HONO})$ ,  $j(\text{HCHO})_M$ ,  
147  $j(\text{HCHO})_R$ ,  $j(\text{H}_2\text{O}_2)$ ) were calculated from solar actinic flux spectra measured by a  
148 spectroradiometer as described by Bohn et al. (Bohn et al., 2008). The particle number  
149 size distributions were measured by a system consisting of a Nano-SMPS (TSI  
150 DMA3085 + CPC3776) and a SMPS (TSI DMA3081 + CPC3775). Aerosol surface  
151 concentration ( $S_a$ ) during 2006–2016 was calculated from the measured particle number  
152 size distributions between 3 nm and 700 nm by assuming the particles are spherical in  
153 shape.

## 154 **2.2 Estimate of photolysis frequencies**

155 Photolysis frequencies were measured in August 2011–2014 and 2016. The  
156 Tropospheric Ultraviolet and Visible (TUV) radiation model (version 5.3) was used to  
157 calculate photolysis frequencies in August over the entire 2006–2016 period under  
158 clear-sky conditions. TUV uses the discrete-ordinate algorithm (DISORT) with four  
159 streams and calculates the actinic flux spectra with a wavelength range of 280 – 420 nm  
160 in 1 nm steps and resolution. We used observed aerosol optical properties including  
161 AOD, single scattering albedo (SSA) and Ångström exponent (AE), total ozone column  
162 to constrain the TUV model (Madronich, 1993). The calculated values agree well with  
163 measured results as shown in Figure 1 indicating that the TUV model accurately  
164 calculated the photolysis frequencies. Data of photolysis frequencies under cloudless  
165 conditions were selected according to the presence of AOD data since AOD  
166 measurements were not possible under cloudy conditions.



167

### 168 **2.3 Measurements of aerosol optical properties**

169 Aerosol optical properties were measured with a CIMEL Sun photometer  
170 (AERONET level 1.5 and level 2.0 data collection, <http://aeronet.gsfc.nasa.gov/>) at the  
171 Beijing-CAMS site (39.933°N, 116.317°E) and at the Beijing site (39.977N,116.381E).  
172 The instrumentation, data acquisition, retrieval algorithms and calibration procedure,  
173 which conform to the standards of the AERONET global network, are described in  
174 detail by Fottiadi et al. (Fottiadi et al., 2006). The solar extinction measurements taken  
175 every 3 minutes within the spectral range 340 – 1020 nm were used to compute AOD  
176 at 340, 380, 440, 500, 675, 870, 970 and 1020 nm. The overall uncertainty in AOD data  
177 under cloud-free conditions was 0.02 at a wavelength of 440 nm (Dubovik and King,  
178 2000). In this study, AOD at the wavelength of 380nm was chosen for analysis. This  
179 wavelength was selected as it is more representative of  $j(\text{NO}_2)$ . In addition to AOD, that  
180 network also provided single scattering albedo (SSA) and Ångström exponent (AE)  
181 data.

182 Cloud optical thickness (COT) was acquired from Aura satellite measurements  
183 with a time resolution of 24 hours. Total ozone column was obtained by OMI (Ozone  
184 Monitoring Instrument), using overpass data.

### 185 **2.4 Chemical box model**

186 Ozone production rate,  $P(\text{O}_3)$ , is calculated by a chemical box model. This model  
187 is based on the compact Regional Atmospheric Chemical Mechanism version 2  
188 (RACM) described by Goliff et al. (Goliff et al., 2013), which includes 17 stable  
189 inorganic species, 4 inorganic intermediates, 55 stable organic compounds and 43  
190 intermediate organic compounds. Compounds that are not explicitly treated in the  
191 RACM are lumped into species with similar functional groups. The isoprene  
192 mechanism includes a more detailed mechanism based on the Leuven Isoprene  
193 Mechanism (LIM) proposed by Peeters et al. (Peeters et al., 2009). A detailed



194 description of this model can be found in Tan et al. (Tan et al., 2017).

195 In this study, the model was constrained by measured hourly average CO, NO<sub>2</sub>,  
196 O<sub>3</sub>, SO<sub>2</sub>, NMHCs (56 species), HCHO, photolysis frequencies, temperature, pressure,  
197 and relative humidity. HONO was not measured. HONO concentrations are generally  
198 underestimated by the gas phase reaction source of HONO (OH + NO → HONO) in  
199 urban areas due to the emission of HONO and the heterogeneous reaction of NO<sub>x</sub> at  
200 surfaces to form HONO, both of which are related to NO<sub>x</sub> concentration. As a result,  
201 the HONO concentration was calculated according to the concentration of NO<sub>2</sub> and  
202 the observed ratio of HONO to NO<sub>2</sub> at an urban site in Beijing, which had a marked  
203 diurnal cycle (Hendrick et al., 2014). For the model calculation, the ratio of HONO to  
204 NO<sub>2</sub> is equal to 0.08 at 6:00 and decreases linearly from 0.08 to 0.01 during 6:00 -  
205 10:00 reflecting increasing photolysis of HONO, and maintains the value of 0.01  
206 during 10:00-18:00. In this study, we focused on daytime P(O<sub>3</sub>) (6:00 - 18:00), thus  
207 the nocturnal HONO concentrations were not required.

208 RO<sub>2</sub>, HO<sub>2</sub>, OH were simulated by the box model to calculate the ozone  
209 production rate as shown in Equation E1 and E2 as derived by Mihelcic et al.  
210 (Mihelcic et al., 2003).

$$211 \quad P(O_3) = k_{HO_2+NO} [HO_2][NO] + \sum (k^i_{RO_2+NO} [RO_2^i][NO]) - k_{OH+NO_2} [OH][NO_2] - L(O_3) \quad E1$$

$$212 \quad L(O_3) = (\theta j(O^1D) + k_{OH+O_3} [OH] + k_{HO_2+O_3} [HO_2] + \sum (k^j_{alkene+O_3} [alkene^j][O_3]) \quad E2$$

213 where  $\theta$  is the fraction of O<sup>1</sup>D from ozone photolysis that reacts with water vapor.  $i$  and  
214  $j$  represent the number of species of RO<sub>2</sub> and alkenes, respectively.

215 The model runs were performed in a time-dependent mode with two days' spin-  
216 up. A 24 h lifetime was introduced for all simulated species, such as secondary species  
217 and radicals, to approximately simulate dry deposition and other losses of these  
218 species (Lu et al., 2013). This lifetime corresponds to an assumed deposition velocity  
219 of 1.2 cm s<sup>-1</sup> and a well-mixed boundary layer height of about 1 km. Sensitivity tests  
220 show that this assumed deposition lifetime has a relatively small influence on the  
221 reactivity of modeled oxidation products and RO<sub>x</sub> radicals.

222 Aerosols can influence O<sub>3</sub> production by heterogeneous reactions such as uptake



223 of HO<sub>2</sub>, NO<sub>2</sub>, N<sub>2</sub>O<sub>5</sub> and NO<sub>3</sub>. For these species, the heterogeneous uptake of HO<sub>2</sub> is  
224 expected to have the largest effect on rapid ozone production in summertime and VOC-  
225 limited conditions (Li et al., 2019). Thus, the effect of heterogeneous reaction of HO<sub>2</sub>  
226 on ozone production was simulated in the chemical box model using RH corrected  
227 aerosol surface concentration (S<sub>aw</sub>) and uptake coefficient of HO<sub>2</sub>. The rate of change  
228 in HO<sub>2</sub> due to irreversible uptake is expressed by E3.

$$229 \quad \frac{dC}{dt} = \frac{\gamma_{HO_2} \times S_{aw} \times v \times C}{4} \quad E3$$

230 Where C, v, and  $\gamma_{HO_2}$  are the gas phase concentration, mean molecular velocity, and  
231 uptake coefficient, respectively. To derive S<sub>aw</sub> we used the measured hygroscopic  
232 factor (Liu et al., 2009) and measured RH to correct the measurement-derived S<sub>a</sub> to  
233 ambient conditions. In this study, we chose  $\gamma_{HO_2} = 0.2$  provided by laboratory  
234 measurements of HO<sub>2</sub> uptake by aerosol particles collected at two mountain sites in  
235 eastern China (Taketani et al., 2012). The effects of HO<sub>2</sub> uptake on P(O<sub>3</sub>) in Beijing in  
236 2006 were simulated assuming that the product of HO<sub>2</sub> uptake by aerosols is either  
237 H<sub>2</sub>O or H<sub>2</sub>O<sub>2</sub>. The results indicate that the two scenarios showed no significant  
238 difference because the recycling of HO<sub>x</sub> radicals from H<sub>2</sub>O<sub>2</sub> is inefficient (Li et al.,  
239 2019). In the following simulations in this study, the product of HO<sub>2</sub> uptake by  
240 aerosols is taken to be H<sub>2</sub>O.

## 241 **3 Results and discussion**

### 242 **3.1 Trend of ozone**

243 Ozone pollution levels can be characterized by a number of metrics. Table 2 lists  
244 10 ozone metrics and their definition summarized by Lu et al. (Lu et al., 2018). We  
245 classify these indicators into four categories: (1) metrics that characterize general levels  
246 of ozone: median value of hourly ozone concentrations (median), daily maximum 8 h  
247 average ozone concentration (MDA8) and daytime average ozone concentration  
248 (DTA<sub>8</sub>); (2) metrics that characterize extreme levels of ozone: daily maximum 1 h



249 average ozone concentration (MDA1), 98th percentile of hourly ozone concentrations  
250 (Perc98) and 4th highest MDA8 (4MDA8); (3) metrics that characterize ozone  
251 exposure: cumulative hourly ozone concentrations of >40 ppb (AOT40) and sum of  
252 positive differences between MDA8 and a cutoff concentration of 35 ppb (SOMO35);  
253 (4) The metrics that characterize the days when the ozone exceeds the standard: total  
254 number of days with MDA8 values of >70 ppb (NDGT70) and number of days with  
255 the ozone concentration exceeding the Chinese grade II national air quality standard  
256 (Exceedance). Figure 2 presents variations in these four categories of ozone metrics at  
257 PKUERS site during the study periods. The results show that overall all metrics  
258 increased during the 12 year period. However, the percent increase and the correlation  
259 coefficient of each metric are different. The median, DTAvg, and MDA8 indicators,  
260 which characterize the general concentration levels of ozone, had an increase rate of  
261 2.8% ~ 5.7% yr<sup>-1</sup>. The metrics that characterize the extreme concentration levels of  
262 ozone had a slower increase rate of 1.2% ~ 2.7% yr<sup>-1</sup>. Among them, Perc98 had the  
263 smallest rise rate, only 1.2% yr<sup>-1</sup>, and the correlation is not significant ( $r^2 = 0.11$ ). This  
264 suggests that the extreme ozone pollution increased much less significantly. In contrast,  
265 the increase rates of the ozone exposure metrics AOT40 and SOMO35 was are faster,  
266 8.4% yr<sup>-1</sup> and 8.3% yr<sup>-1</sup>, respectively, than the metrics that characterize ozone  
267 concentrations. The NDGT70 and Exceedance metrics, related to the number of days  
268 of ozone exceeding the standard, showed the fastest increases, 10% yr<sup>-1</sup> and 9.8% yr<sup>-1</sup>,  
269 respectively. It worth noting that most of metrics decreased significantly from 2014 to  
270 2016 except for Perc98 and 4MDA8.

271 As shown in Figure 3, from 2005 to 2016 MDA8 O<sub>3</sub> concentrations increased at a  
272 rate of  $2.3 \pm 1.2$  ppbv ( $3.3 \pm 1.8$  %) yr<sup>-1</sup> ( $r^2 = 0.66$ ) at the PKUERS site, which  
273 corresponds to a total MDA8 ozone increase of 25.3 ppbv. Meanwhile, O<sub>x</sub> (O<sub>3</sub>+NO<sub>2</sub>)  
274 concentrations increased at a slower rate of  $1.4 \pm 0.6$  ppbv ( $1.9 \pm 0.8$  %) yr<sup>-1</sup>, due to the  
275 decrease in NO<sub>x</sub> concentrations (second graph in Figure 2).

276 Temperature and wind speed, which can directly influence ozone production and  
277 concentrations, showed no significant trend during 2005-2016 (Figure 4). The average



278 temperatures in summer were between 26 and 31°C. The temperature in 2005 was the  
279 lowest and in 2007 it was the highest. The average wind speeds were less than 2.5 m s<sup>-1</sup>  
280 <sup>1</sup> in all years. The average relative humidity may have decreased slightly (~ 1.5% yr<sup>-1</sup>).  
281 In summary, we believe that meteorological factors did not play more than a minor role  
282 in the overall Beijing O<sub>3</sub> trend. Therefore, our discussion focuses on photochemical  
283 processes.

284 The ozone concentration observed at a receptor site depends on two contributions:  
285 regional background ozone and local photochemical production. We have no direct  
286 measurements of the long-term trend of regional background ozone in Beijing, but  
287 others have reported measurements of ozone at regional background sites in China. At  
288 a baseline Global Atmospheric Watch (GAW) station in the northeastern Tibetan  
289 Plateau region (Mt Waliguan, 36.28° N, 100.9° E) the average annual daytime ozone  
290 concentration increased at a rate of 0.24 ppb yr<sup>-1</sup>, over the 1994 to 2013 period, but  
291 there was no significant trend in summer (Xu et al., 2018). The measurement at a rural  
292 station in Beijing (116.22° E, 40.29° N, 34 km northwest of the observation site in this  
293 study) showed a decrease of ozone at a rate of -0.47 ppb yr<sup>-1</sup> over the 2004 to 2015  
294 period (Zheng et al., 2016). The MDA8 ozone concentration at the Shangdianzi site, a  
295 background station in northern China, showed an increasing trend of 1.1 ppb yr<sup>-1</sup> during  
296 2004-2014 (Ma et al., 2016a). Additionally, there were very small trends of O<sub>3</sub>  
297 concentrations at the background site (Dongtan) in Shanghai, located in the southern  
298 North China Plain (Gao et al., 2017). Based on these reports of smaller and variable  
299 trends, we assume that the trend in regional background ozone in the North China Plain  
300 made only a minor contribution to the ozone trend observed at the PKUERS site (2.3 ±  
301 1.2 ppbv yr<sup>-1</sup>). We thus surmise that the increase in O<sub>3</sub> at the PKUERS site was mainly  
302 due to “local” photochemistry driven by emissions of ozone precursors from downtown  
303 and the surrounding suburban areas of Beijing.

### 304 **3.2 Trend of gaseous precursors**

305 This increase in ozone concentrations is opposite to the decreasing trend of its



306 precursors, including VOCs, CO and NO<sub>x</sub> (Figure 5). The overall change of the total  
307 OH loss rate due to VOCs (VOC reactivity) was  $-0.36 \text{ s}^{-1}$  ( $-6.0\%$ )  $\text{yr}^{-1}$ . For  
308 anthropogenic VOCs, the highest reactivity was generally contributed by alkene  
309 species, with an average value over the eleven years of  $2.00 \pm 0.43 \text{ s}^{-1}$ , followed by  
310 aromatics and alkanes, with average reactivities of  $1.51 \pm 0.74 \text{ s}^{-1}$  and  $0.92 \pm 0.60 \text{ s}^{-1}$ ,  
311 respectively. Thus, the alkenes and aromatics are more important for O<sub>3</sub> production  
312 than are alkanes. The trends for alkenes, aromatics, and alkanes were a decrease of  
313  $0.14 \text{ s}^{-1}$  (7.1%),  $0.12 \text{ s}^{-1}$  (7.9%), and  $0.065 \text{ s}^{-1}$  (7.0%)  $\text{yr}^{-1}$ , respectively, indicating that  
314 alkenes and aromatics played the dominant role in the reduction of anthropogenic  
315 VOC reactivity. The rate of decrease in VOCs at PKUERS site is similar to that  
316 reported for Los Angeles by Warneke et al. and Pollack et al. ( $7.3\text{--}7.5\%$   $\text{yr}^{-1}$  over 50  
317 years) (Warneke et al., 2012; Pollack et al., 2013). The decrease in anthropogenic  
318 VOCs in Los Angeles was predominantly attributed to decreasing emissions from  
319 motor vehicles due to increasingly strict emissions standards. Similarly, a previous  
320 study at the PKUERS site indicated that the decreasing anthropogenic VOC was  
321 mainly attributed to the reduction of gasoline evaporation and vehicular exhaust under  
322 the implementation of stricter emissions standards for new vehicles and specific  
323 control measures for in-use vehicles (Wang et al., 2015a). For naturally emitted  
324 VOCs, mainly isoprene, the OH reactivity had little trend with large fluctuations, as  
325 the emissions of plants vary greatly with temperature and light intensity. Therefore,  
326 the decrease in total VOCs reactivity was dominated by the decrease in anthropogenic  
327 VOCs. Similarly, CO, which is mainly contributed by anthropogenic emissions,  
328 decreased rapidly ( $9.3\%$   $\text{yr}^{-1}$ ) during 2006–2016.

329 Daytime concentrations of NO<sub>x</sub> at the PKUER site also decreased significantly  
330 from 2006 to 2016 (Figure 5), with a slope (excluding 2008, which had a much lower  
331 NO<sub>x</sub> concentration due to enhanced emission controls implemented during the Olympic  
332 Games) of  $-1.48 \text{ ppbv yr}^{-1}$  ( $-5.5\%$   $\text{yr}^{-1}$ ,  $r^2 = 0.81$ ). The decrease in NO<sub>x</sub> was mainly  
333 due to the reduction in vehicle exhaust and coal combustion (Zhao et al., 2013). The  
334 decrease in NO<sub>x</sub> was significantly faster than that found in Los Angeles by Pollack et



335 al. (2.6% yr<sup>-1</sup> over 50 years) (Pollack et al., 2013). In contrast to Beijing, Los Angeles  
336 O<sub>3</sub> concentrations have continuously decreased from 1980 to 2010 (Parrish et al., 2016).  
337 The ratio of the rates of decrease of VOCs and NO<sub>x</sub> in Los Angeles (2.9) is significantly  
338 greater than unity and larger than that at the PKUER site (1.1), which possibly can be  
339 a contributing cause of the opposite trends of ozone in the two regions. It worth noting  
340 that the precursor concentrations in 2008, the Olympic Games year, were particularly  
341 low, but that ozone was nevertheless on the regression line. The monthly average ratio  
342 of VOC reactivity to NO<sub>x</sub> concentration in 2008 is 0.28 s<sup>-1</sup> ppbv<sup>-1</sup>, higher than the  
343 average ratio of VOC reactivity to NO<sub>x</sub> concentration during 2006-2016 (0.24 s<sup>-1</sup> ppbv<sup>-1</sup>).  
344 The adverse reduction ratio of VOC to NO<sub>x</sub> is the main cause of inefficient reduction  
345 in O<sub>3</sub> level in 2008, which is consistent with the study of Chou et al. (2011).

346 Since 2013, under the implementation of the Action Plan on Air Pollution  
347 Prevention and Control ([http://www.gov.cn/zwqk/2013-09/12/content\\_2486773.htm](http://www.gov.cn/zwqk/2013-09/12/content_2486773.htm)),  
348 more stringent emission control measures were implemented to restrict industrial and  
349 vehicle emission. As a result, there are indications that both VOCs and NO<sub>x</sub> decreased  
350 faster over the 2013 to 2016 period: 0.81 s<sup>-1</sup> yr<sup>-1</sup> (16% yr<sup>-1</sup>, r<sup>2</sup> = 0.71) and 1.94 ppbv yr<sup>-1</sup>  
351 (9.3% yr<sup>-1</sup>, r<sup>2</sup> = 0.78) for VOC reactivity and NO<sub>x</sub>, respectively. This could be the  
352 cause of the decline in O<sub>3</sub> concentrations from 2014 to 2016.

### 353 3.3 Trend of particulate matter

354 From 2009 to 2016, PM<sub>2.5</sub> concentrations declined rapidly, achieving the air  
355 quality standard of China (35 µg/m<sup>3</sup>) in 2016 (Figure 6). Since 2000, Beijing had  
356 implemented 16 phases' air pollution control measures, mainly including the  
357 controlling of industry, motor vehicle, coal combustion and fugitive dust pollution,  
358 which was effective for the reduction in PM<sub>2.5</sub> (Lang et al., 2017). Especially the  
359 strengthening of the reduction in coal combustion, which was gradually replaced by  
360 natural gas since 2004, favored improved visibility in Beijing (Zhao et al., 2011).

361 As shown in Figure 6, from 2006 to 2016 AOD decreased at a rate of 9.3% yr<sup>-1</sup>.  
362 The correlation between AOD and PM<sub>2.5</sub> can be determined from the observations of



363 PM<sub>2.5</sub> and AOD in August during 2009-2016 at the PKUERS site (Figure 7). AOD  
364 and PM<sub>2.5</sub> are linearly correlated with a correlation coefficient of +0.74. This result  
365 indicates that the decrease in PM<sub>2.5</sub> was the primary cause of the reduction in AOD. In  
366 addition to PM<sub>2.5</sub>, relative humidity also has an important effect on AOD. The  
367 decrease in relative humidity during 2006-2016 (Figure 4) would reduce the  
368 hygroscopic growth of aerosol, leading to a weakened extinction effect of particulate  
369 matter on solar radiation (Qu et al., 2015). It is worth noting that although PM<sub>2.5</sub> in  
370 2011 was lower than that in 2010, AOD in 2011 was higher than that in 2010 (Figure  
371 6). For one reason, the relative humidity in 2011 was higher. Additionally, the aerosol  
372 type, atmospheric boundary layer height and the vertical structure of aerosol  
373 distribution also affects the dependence of AOD on PM<sub>2.5</sub> (Zheng et al., 2017),  
374 probably contributing to the scatter about the AOD versus PM<sub>2.5</sub> relationship shown in  
375 Figure 7.

376 Monthly mean AE (380/550 nm) in August showed no overall trend during 2006-  
377 2016 (Figure 8). The monthly AE means were between 0.87 and 1.2, suggesting that  
378 the size-distribution of aerosol was generally stable during this period. Monthly mean  
379 SSA (440 nm) in August showed an upward trend of +0.004 yr<sup>-1</sup> (+0.45% yr<sup>-1</sup>) during  
380 2006-2016 (Figure 8), indicating the proportion of the light-absorbing component of  
381 aerosols (e.g. black carbon) has decreased, due to the stringent and effective controls  
382 on the burning of biomass/biofuel and coal (Ni et al., 2014; Cheng et al., 2013). This  
383 result is consistent with the studies of Lang et al. and Wang et al., which indicated that  
384 black carbon in China's mega cities has decreased rapidly over the past decade (Wang  
385 et al., 2016; Lang et al., 2017).

### 386 3.4 Trend of photolysis frequencies

387 The influence of solar radiation on O<sub>3</sub> photochemistry can be described by  
388 actinic flux (or photolysis frequencies). We chose  $j(\text{NO}_2)$  as a representative  
389 photolysis frequency to analyze the trend of actinic flux. Wang et al (2019) studied the  
390 quantitative relationship between  $j(\text{NO}_2)$  and AOD at the PKUERS site, and found



391 that  $j(\text{NO}_2)$  and AOD showed a clear nonlinear negative correlation at a given SZA,  
392 with slopes ranging from -1.3 to  $-3.2 \times 10^{-3} \text{ s}^{-1}$  at  $\text{AOD} < 0.7$ , indicating a significant  
393 extinction effect of AOD on actinic flux near the ground.

394 The  $j(\text{NO}_2)$  calculated by the TUV model under clear-sky conditions shows an  
395 upward trend of  $3.6\% \text{ yr}^{-1}$  from 2005 to 2016 and agrees well with the 5 years of  
396 observed values from 2011 to 2016 (Figure 6). According to sensitivity analysis of  
397 TUV, the decrease in AOD plays a dominant role in the  $j(\text{NO}_2)$  increase, contributing  
398 about 80% of the total. Additionally, the increase in SSA also contributes significantly  
399 to  $j(\text{NO}_2)$  increase, contributing about 17%.

400 In addition to aerosol optical properties, the photolysis frequency in the planetary  
401 boundary layer is affected by other factors, including cloud extinction, ground  
402 reflection, absorption by gases such as  $\text{O}_3$ , and Rayleigh scattering by gases. The  
403 ground reflection is relatively stable for different years in the same city with stable  
404 ground covering. The change in Rayleigh scattering of gases and absorption of  $\text{NO}_2$ ,  
405  $\text{SO}_2$  and HCHO plays a negligible role in the variation in photolysis frequencies  
406 according to sensitivity analysis of TUV model. This is consistent with the results of  
407 Barnard et al. (Barnard et al., 2004). As shown in Figure 9, the total ozone column  
408 fluctuated between 285-307 DU without a significant overall trend. The magnitude of  
409 total ozone column variation (22 DU) can leading  $j(\text{O}^1\text{D})$  changing of about 10%, but  
410 plays a negligible role in changing other photolysis frequencies according to  
411 sensitivity analysis using the TUV model. The cloud optical thickness (COT) for most  
412 years was relatively stable, ranging from 6 to 8, but in 2005, 2012 and 2015 COT was  
413 significantly larger (Figure 9). As there was no significant trend of COT, we surmised  
414 that the light-extinction effect of clouds did not play a key role in changing photolysis  
415 frequencies.

### 416 **3.5 Combined effect of changes in ozone precursors and aerosols on ozone** 417 **production**

418 We investigated the overall effect of the changes in VOCs,  $\text{NO}_x$ , photolysis



419 frequency, and aerosol uptake of HO<sub>2</sub> on ozone production rate using the chemical  
420 box model. By testing the response of P(O<sub>3</sub>) as calculated from Equation E1 to the  
421 changes of VOCs and NO<sub>x</sub> concentrations (Figure 10), we concluded that  
422 photochemical environment of the PKUERS site was, on average, in the VOC-limited  
423 regime. This result is consistent with previous studies (Zhang et al., 2014;Chou et al.,  
424 2011). Under this condition, the long-term decrease in VOCs in Beijing has  
425 contributed to a decrease in P(O<sub>3</sub>), while the decrease in NO<sub>x</sub> has tended to increase  
426 P(O<sub>3</sub>). As shown in Figure 11, when the increase in photolysis frequencies and aerosol  
427 uptake of HO<sub>2</sub> were not included in the calculation, the simulated P(O<sub>3</sub>) decreased  
428 slightly at a rate of 1.1% yr<sup>-1</sup>. This indicates that the ratio of the rates of decrease of  
429 VOCs and NO<sub>x</sub> (about 1.1) is nearly inefficient in reducing ozone production in  
430 Beijing. However, when the increase in photolysis frequencies was included in the  
431 model calculation, the calculated P(O<sub>3</sub>) showed an increasing trend of 2.2% yr<sup>-1</sup>. This  
432 result indicates that the increase in photolysis frequencies more than compensated for  
433 the downward trend of O<sub>3</sub> production driven by decreased VOCs and NO<sub>x</sub>, leading to  
434 increasing O<sub>3</sub> production through the decade. The photochemical box model  
435 calculations indicate that the increase in photolysis frequencies has two major impacts  
436 on P(O<sub>3</sub>) - an increase in primary production of OH through accelerated photolysis of  
437 O<sub>3</sub>, HONO, HCHO and other carbonyl compounds, and an accelerated radical  
438 recycling of OH as VOCs are oxidized. As particulate matter has decreased and  
439 photolysis frequencies correspondingly have increased, a more rapidly decreasing rate  
440 of the VOC to NO<sub>x</sub> ratio is required to achieve a significant reduction in O<sub>3</sub> in the  
441 future.

442 When we include heterogeneous uptake of HO<sub>2</sub> in the model, the calculated  
443 P(O<sub>3</sub>) increases at the faster rate of 2.9% yr<sup>-1</sup> due to the overall reduced aerosol  
444 surface concentration (S<sub>a</sub>) and thus the reduced heterogeneous uptake of HO<sub>2</sub> (Figure  
445 11). This result indicates that the effect of heterogeneous uptake of HO<sub>2</sub> contributed  
446 roughly 0.7% yr<sup>-1</sup> of ozone increase. Hence, our result indicates that the increase in  
447 photolysis rates due to PM decrease plays a more important role than the decrease in



448 heterogeneous uptake of HO<sub>2</sub> by aerosols in accelerating ozone production in Beijing.  
449 Previous measurements indicate that the uptake coefficient varies widely from 0.003  
450 to 0.5 with a strong dependence on the aerosol concentration of transition metal ions  
451 such as Cu(II) (Zou et al., 2019;Taketani et al., 2008;Lakey et al., 2015;Matthews et  
452 al., 2014;Lakey et al., 2016). This strong dependence on aerosol composition implies  
453 that a single assumed value for  $\gamma_{\text{HO}_2} = 0.2$  has large uncertainty.  $\gamma_{\text{HO}_2} = 0.2$  used in our  
454 simulation is likely an overestimate of the effect of heterogeneous uptake of HO<sub>2</sub> on  
455 ozone production rate at PKUERS site.

456 In summertime PM in the Beijing urban area is mainly formed by the secondary  
457 conversion of gaseous precursors (Han et al., 2015;Guo et al., 2014), indicating that  
458 VOCs and NO<sub>x</sub> are not only the precursors of ozone, but also the main precursors of  
459 PM in this urban area. In addition, observations in Beijing have shown that the  
460 secondary components of PM, including secondary organic matter, ammonium sulfate  
461 and ammonium nitrate, dominate the light extinction of PM (Han et al., 2014;Han et al.,  
462 2017;Wang et al., 2015b). As a result, reductions of VOCs and NO<sub>x</sub> are expected to  
463 lead to a decrease in secondary PM formation, and thus to further enhancement in solar  
464 radiation (or actinic flux). Therefore, in order to reduce ozone effectively, the  
465 contribution of VOCs and NO<sub>x</sub> to secondary PM formation and thus their effect on  
466 solar radiation must be comprehensively considered. However, the summertime  
467 formation of PM is quite complex; the conversion efficiency of gaseous precursors to  
468 aerosols and in turn influence ozone production is a research area that requires further  
469 study.

### 470 **3.6 Additional considerations**

471 One limitation of this study is that the photochemical box model is constrained  
472 by surface observations, and hence may not accurately represent some aspects of the  
473 photochemistry through the full depth of the planetary boundary layer over Beijing.  
474 Here we briefly consider several of these aspects: (1) The treatment of ozone and  
475 VOC and NO<sub>x</sub> precursor concentrations likely are accurately represented, because



476 rapid daytime vertical mixing ensures that there is only a small vertical gradient in the  
477 concentrations of these relatively long lived species. (2) In daytime, the HONO  
478 lifetime is so short that it may be largely confined to near the surface, where it has  
479 surface sources (heterogeneous reaction of H<sub>2</sub>O and NO<sub>2</sub> and emissions on surfaces).  
480 Therefore, the estimated HONO based on near-surface NO<sub>2</sub> concentrations may  
481 overestimate average boundary layer HONO concentrations; however in this study the  
482 influence of HONO on the calculation is relatively small, so this is not a large source  
483 of error. (3) The model is constrained by surface measurements of photolysis  
484 frequencies, but these surface measurements do not accurately quantify the actinic  
485 flux throughout the boundary layer. Figure 12 presents the vertical profiles of  $j(\text{NO}_2)$   
486 simulated by the TUV model for aerosol properties representative of Beijing. A thick  
487 layer of aerosol effectively reduces radiation at the bottom of the layer, but not at the  
488 top, where radiation may be enhanced due to upward scattering from the aerosol  
489 below (Dickerson et al., 1997; Jacobson, 1998). Overall, vertical average  $j(\text{NO}_2)$   
490 increased by 32% from 2006 to 2016, which is comparable to the surface increase  
491 (36%). These simulations indicate that the increased trend of  $j(\text{NO}_2)$  derived from  
492 surface observations do approximate the trend through the entire boundary layer.

#### 493 **4 Conclusion**

494 During the past decade, China has devoted very substantial resources to  
495 improving the environment. These efforts have improved atmospheric particulate  
496 matter loading, but ambient ozone levels have continued to increase. Based on the  
497 long-term measurements at a representative site in Beijing, we explored the factors  
498 driving the increase in ozone production. Consistent with the implementation of  
499 stringent emission control measures, concentrations of PM<sub>2.5</sub> and ozone precursors  
500 (VOCs and NO<sub>x</sub>) decreased rapidly, but in contrast O<sub>3</sub> and Ox increased. This  
501 investigation finds that the primary cause of the O<sub>3</sub> increase is that decreasing PM  
502 concentrations led to an increase in actinic flux, which in turn increased the



503 photochemical production of ozone. This result indicates that the influence of aerosol  
504 on ozone production is important for determining the full manifold of atmospheric  
505 effects that result from reducing the emissions of the O<sub>3</sub> and PM precursors.

506

507

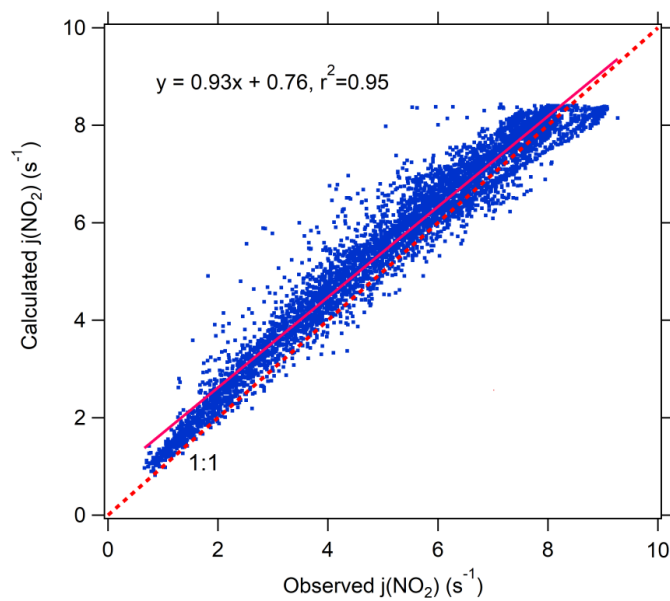
508

## 509 **ACKNOWLEDGEMENTS**

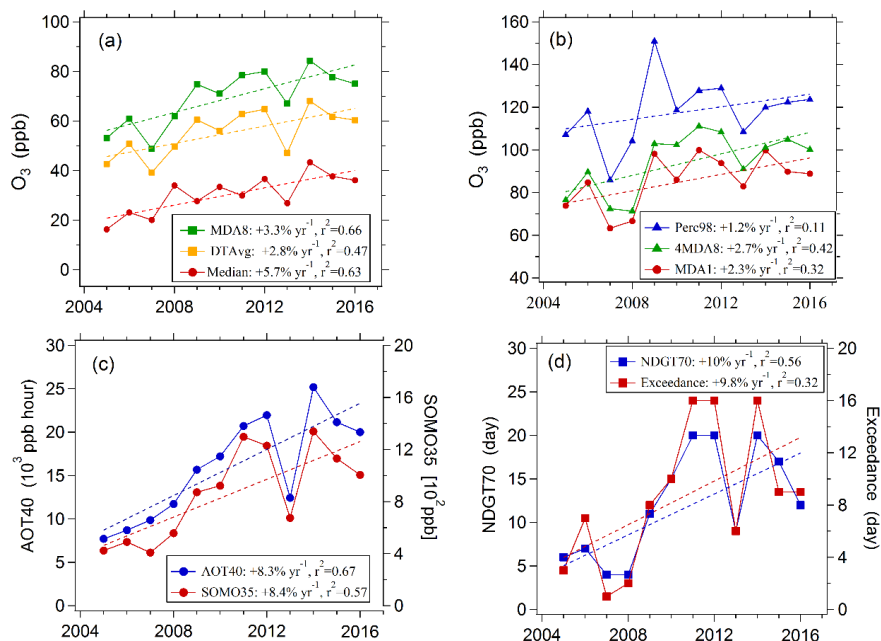
510 This work was supported by the Major Program of the National Natural Science  
511 Foundation of China [Grant number 91644222]. We thank Hongbin Chen and  
512 Philippe Goloub for data management of AOD and other aerosol optical properties on  
513 AERONET.  
514



515  
516  
517  
518  
519  
520  
521



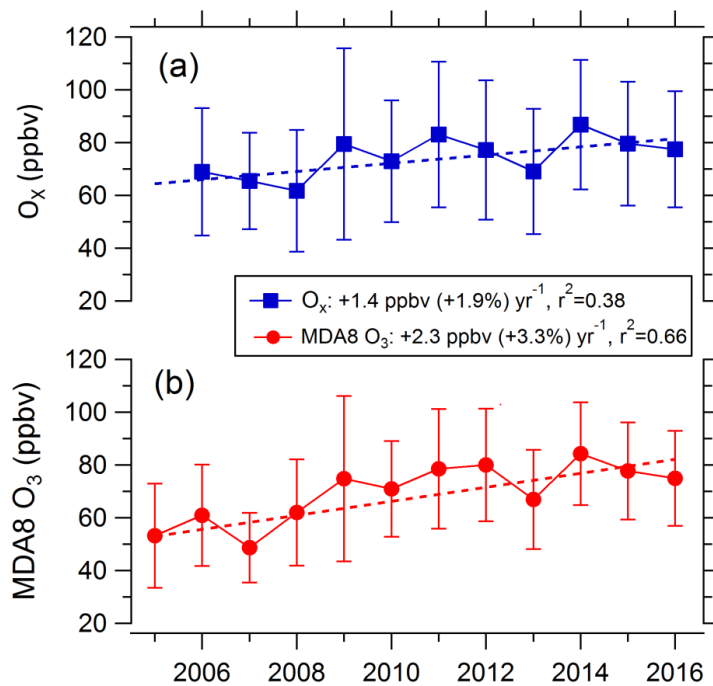
522  
523 Figure 1. Correlation between Observed and calculated  $j(\text{NO}_2)$  by TUV model in  
524 Beijing in summer time during 2012 - 2015.  
525



526  
 527 Figure 2. Variations in multiple O<sub>3</sub> metrics at the PKUERS site in Beijing in August  
 528 between 2005 and 2016.  
 529  
 530



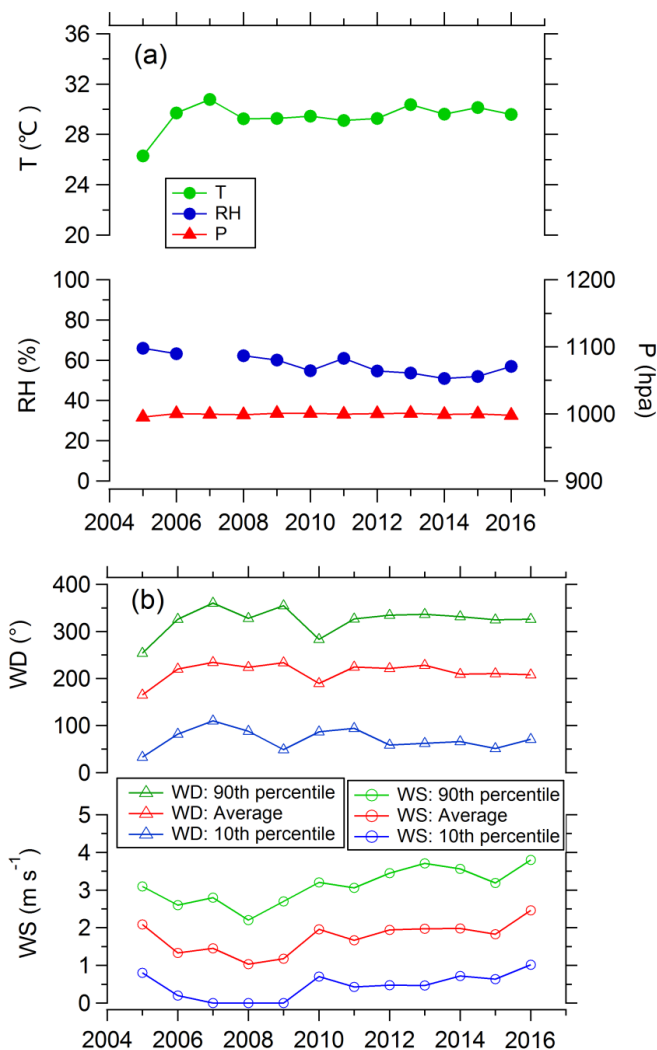
531



532

533 Figure 3. Variations in average MDA8 O<sub>3</sub> and daytime (7:00-19:00) average Ox in  
534 Beijing, August between 2005 and 2016.

535

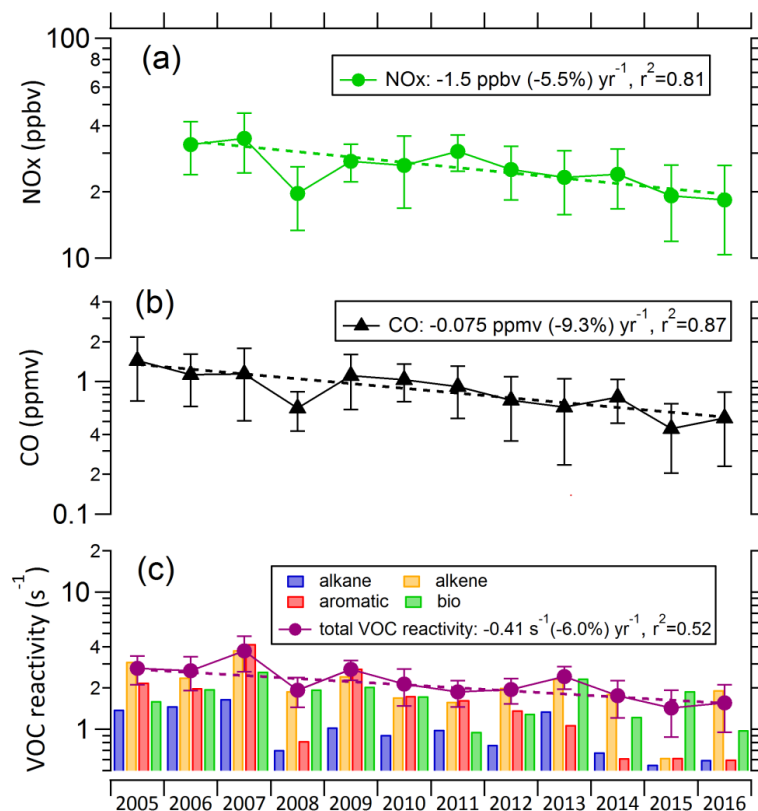


536  
537 Figure 4. Variations in daytime (7:00-19:00) averages of meteorological conditions  
538 including temperature (T), relative humidity (RH), wind direction (WD) and wind  
539 speed (WS) in Beijing, August during 2005 - 2016.  
540



541

542



543

544 Figure 5. Variations in arithmetic mean MDA8 O<sub>3</sub>, arithmetic mean of daytime (7:00-

545 19:00) Ox and geometric mean of daytime NO<sub>x</sub>, CO and VOCs reactivity in Beijing,

546 August between 2005 and 2016. VOCs reactivity is depicted by reactivity of each

547 species (left axis) and total VOC reactivity (right axis). On the y-axes, a linear scale is

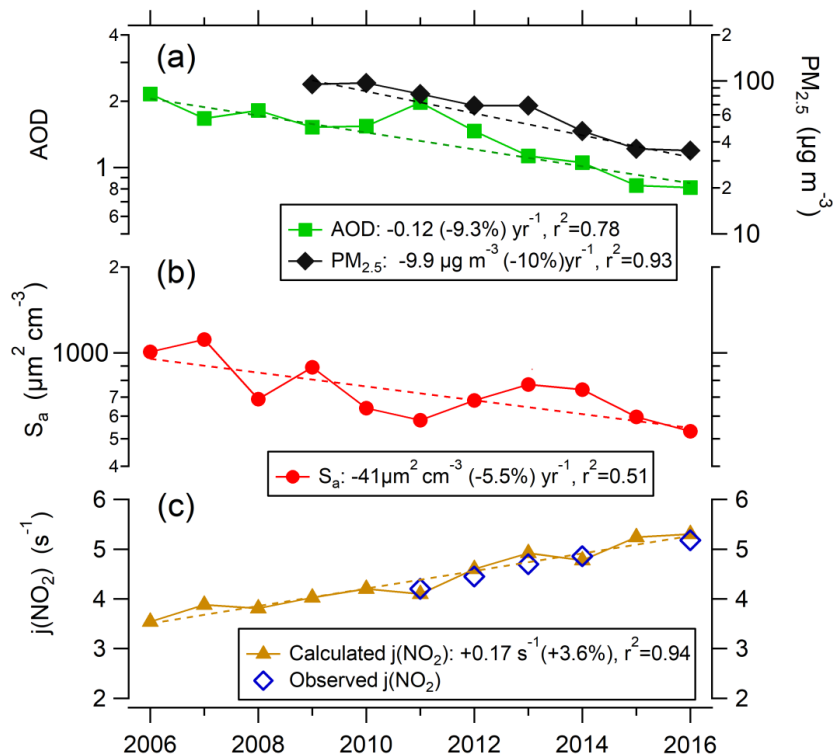
548 used for O<sub>3</sub> and Ox, and a log-scale is used for the precursor concentrations (NO<sub>x</sub>,

549 CO and VOCs).

550



551



552

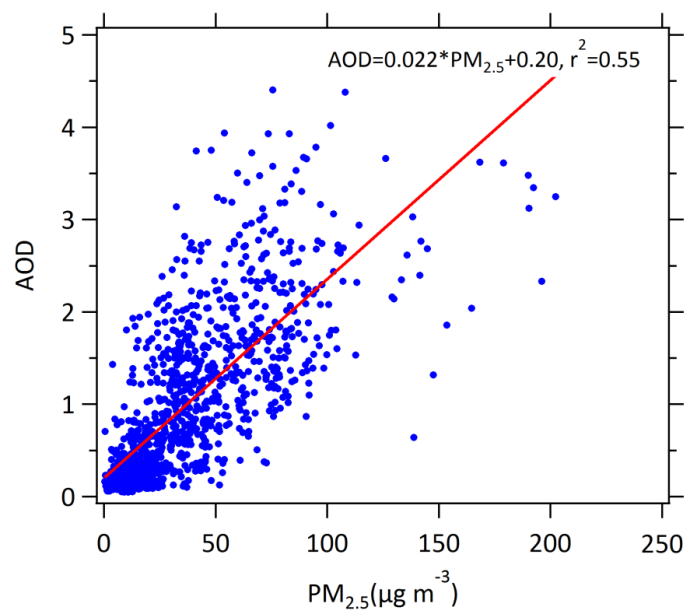
553 Figure 6. Variations in daytime (7:00-19:00) averages of AOD, PM<sub>2.5</sub>, S<sub>a</sub>, j(NO<sub>2</sub>)  
554 Calculated j(NO<sub>2</sub>) by TUV in Beijing, August between 2006 and 2016. AOD and  
555 j(NO<sub>2</sub>) are both corresponding to cloudless weather. On the y-axes, a log-scale is used  
556 for PM<sub>2.5</sub>, AOD and S<sub>a</sub> and a linear scale is used for j(NO<sub>2</sub>).

557

558



559  
560



561

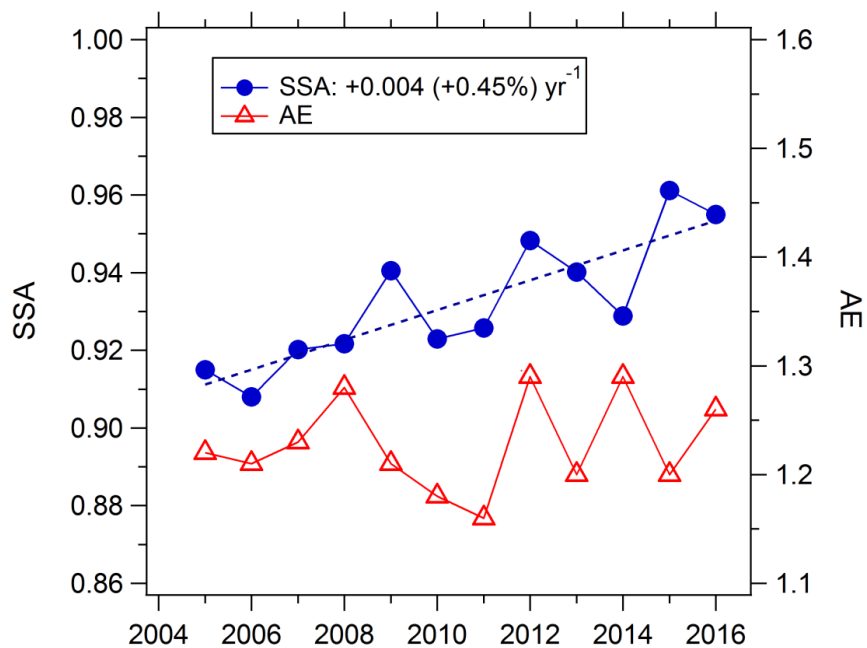
562 Figure 7. Correlation between AOD and PM<sub>2.5</sub> in Beijing, summertime during 2009 -

563 2016.

564



565



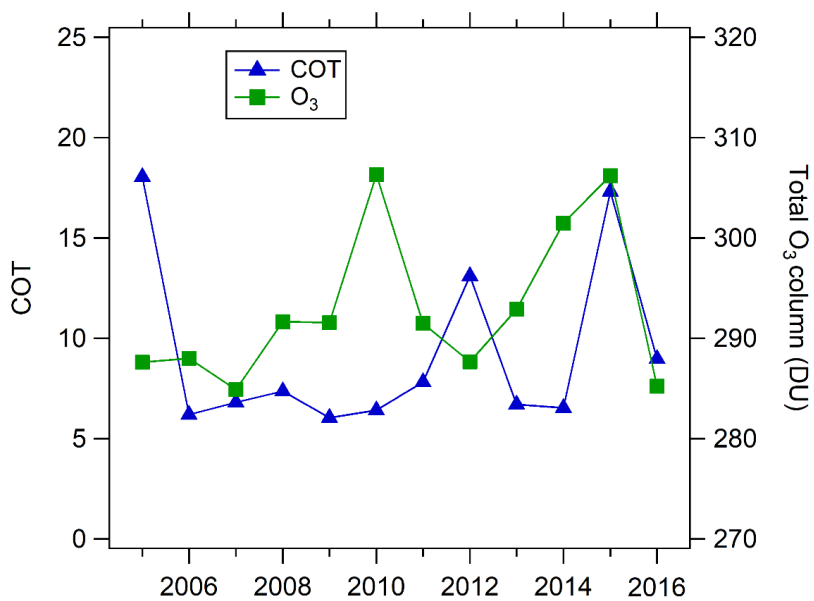
566

567 Figure 8. Variation in monthly mean single scattering albedo (SSA) and Ångström  
568 exponent (AE) in Beijing for the month of August during 2005 - 2016.

569

570

571



572

573 Figure 9. Variations in mean total ozone column and cloud optical thickness (COT) in

574 Beijing for the month of August during 2005 - 2016.

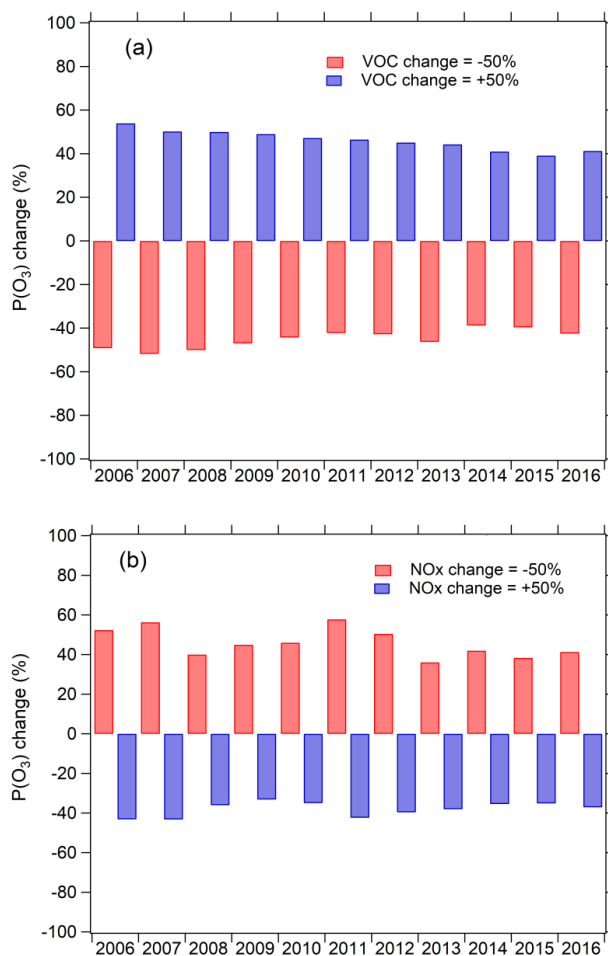
575

576

577



578

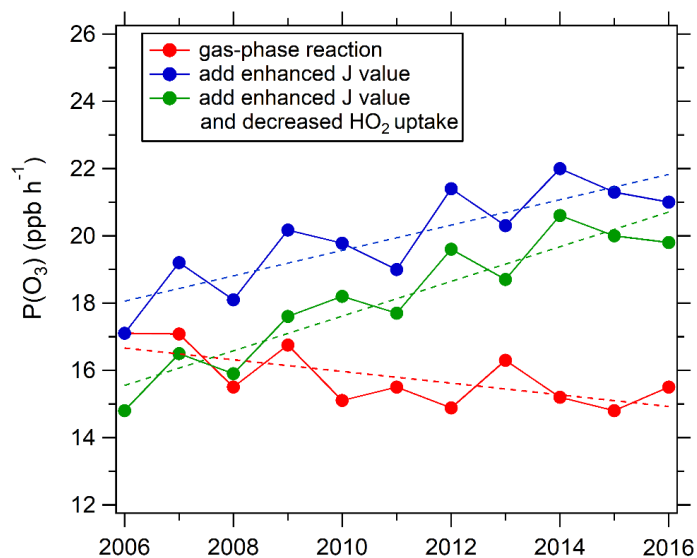


579

580 Figure 10. Sensitivity of monthly daytime mean  $P(O_3)$  to VOCs and  $NO_x$  simulated  
581 by box model during 2006 - 2016. VOCs and  $NO_x$  is increased by 50% or decreased  
582 by 50% to test the fractional change of monthly daytime mean  $P(O_3)$ .  
583



584  
585  
586



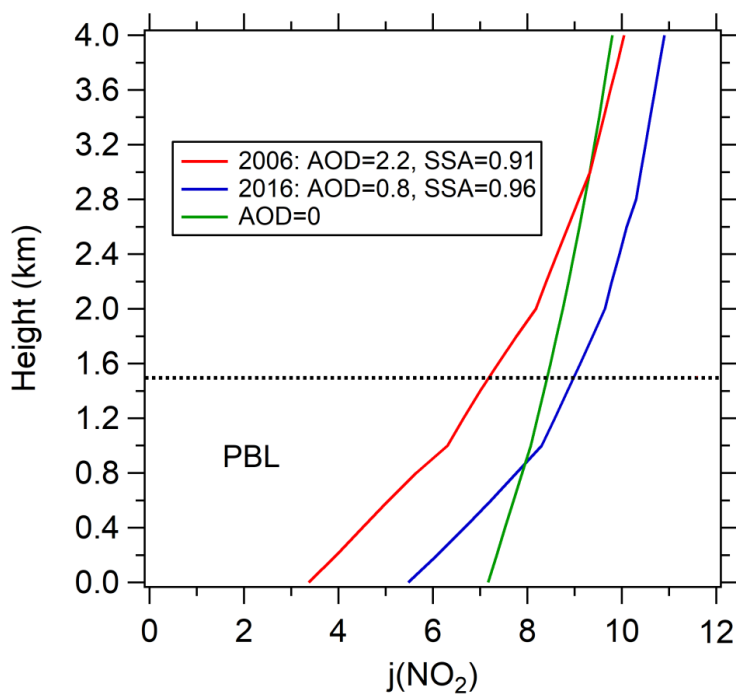
587

588 Figure 11. Trend of monthly daytime mean  $P(\text{O}_3)$  simulated by the chemical box  
589 model. Red dots: Only the gas-phase reactions are considered in the box model  
590 constrained by observed photolysis frequencies from 2006 for all eleven years. Blue  
591 dots: the box model as above, but constrained by the photolysis frequencies derived  
592 for each year. Green dots: the box model constrained by the photolysis frequencies  
593 derived for each year with the changing aerosol uptake of  $\text{HO}_2$  also considered.

594



595  
596



597  
598 Figure 12. Vertical profiles of  $j(\text{NO}_2)$  simulated by the TUV model in Beijing. Three  
599 scenarios are simulated: The model parameters are: (1) AOD=2.2, SSA=0.91 in August  
600 2006; (2) AOD=0.8, SSA=0.96 in August 2016; (3) AOD=0. The daytime average  
601  $\text{SZA}=53^\circ$  is used for all simulations. Dotted line represent the top of boundary layer.  
602  
603



604  
605  
606  
607  
608  
609  
610

611 Table 1. Instruments deployed in the measurement undertaken in August during 2005 -  
612 2016 and used for data analysis.

Parameters	Measurement technique	Time resolution	Detection limit	Accuracy
Photolysis frequencies	Spectroradiometer	10 s	/	± 10%
O <sub>3</sub>	UV photometry	60 s	0.5 ppbv	± 5%
NO	Chemiluminescence	60 s	60 pptv	± 20%
NO <sub>2</sub>	Chemiluminescence	60 s	300 pptv	± 20%
CO	IR photometry	60 s	4 ppb	± 5%
SO <sub>2</sub>	Pulsed UV fluorescence	60 s	0.1 ppbv	± 5%
HCHO	Hantzsch fluorimetry	60 s	25 pptv	± 5%
C2-C10VOCs	GC-FID/MS	1 h	20-300 pptv	± 15~20%
PM <sub>2.5</sub>	TH-2000	60s	1µg m <sup>-3</sup>	± 5%
S <sub>a</sub>	SMPS	60s	/	±3%
AOD, SSA, AE	CIMEL Sun photometer	5min	0.01	±5%

613  
614



615

616

617

618

619

620

621 Table 2. Description of Ozone Metrics used in this study.

categories	metric	definition
general level	median (ppb)	50th percentile of hourly concentrations
	MDA8 (ppb)	daily maximum 8 h average; the mean MDA8 O <sub>3</sub> in August of each year is used in this study.
	DTAvg (ppb)	daytime average ozone is the average of hourly ozone concentrations for the 12 h period from 07:00 to 19:00 local time
extreme level	MDA1 (ppb)	daily maximum 1 h average; the mean MDA1 O <sub>3</sub> in August of each year is used in this study.
	Perc98 (ppb)	98th percentile of hourly concentrations
	4MDA8 (ppb)	4th highest MDA8
ozone exposure	AOT40 (ppb h)	cumulative hourly ozone concentrations of >40 ppb
	SOMO35 (ppb day)	sum of positive differences between MDA8 and a cutoff concentration of 35 ppb
Exceedance days	NDGT70 (day)	total number of days with MDA8 values of >70 ppb
	Exceedance (day)	number of days with the ozone concentration exceeding the Chinese grade II national air quality standard, defined as $MDA8 > 160 \mu\text{g m}^{-3}$

622

623



## 624 Reference

- 625 Atkinson, R.: Atmospheric chemistry of VOCs and NO<sub>x</sub>, *Atmospheric Environment*,  
626 34, 2063-2101, 2000.
- 627 Barnard, J. C., Chapman, E. G., Fast, J. D., Schmelzer, J. R., Slusser, J. R., and Shetter,  
628 R. E.: An evaluation of the FAST-J photolysis algorithm for predicting nitrogen  
629 dioxide photolysis rates under clear and cloudy sky conditions, *Atmospheric*  
630 *Environment*, 38, 3393-3403, <https://doi.org/10.1016/j.atmosenv.2004.03.034>,  
631 2004.
- 632 Bohn, B., Corlett, G. K., Gillmann, M., Sanghavi, S., Stange, G., Tensing, E.,  
633 Vrekoussis, M., Bloss, W. J., Clapp, L. J., Kortner, M., Dorn, H. P., Monks, P. S.,  
634 Platt, U., Plass-Dulmer, C., Mihalopoulos, N., Heard, D. E., Clemitshaw, K. C.,  
635 Meixner, F. X., Prevot, A. S. H., and Schmitt, R.: Photolysis frequency  
636 measurement techniques: results of a comparison within the ACCENT project,  
637 *Atmospheric Chemistry and Physics*, 8, 5373-5391, 10.5194/acp-8-5373-2008,  
638 2008.
- 639 Castro, T., Madronich, S., Rivale, S., Muhlia, A., and Mar, B.: The influence of aerosols  
640 on photochemical smog in Mexico City, *Atmospheric Environment*, 35, 1765-  
641 1772, [https://doi.org/10.1016/S1352-2310\(00\)00449-0](https://doi.org/10.1016/S1352-2310(00)00449-0), 2001.
- 642 Cheng, Y., Engling, G., He, K. B., Duan, F. K., Ma, Y. L., Du, Z. Y., Liu, J. M., Zheng,  
643 M., and Weber, R. J.: Biomass burning contribution to Beijing aerosol, *Atmos.*  
644 *Chem. Phys.*, 13, 7765-7781, 10.5194/acp-13-7765-2013, 2013.
- 645 Chou, C. C. K., Tsai, C. Y., Chang, C. C., Lin, P. H., Liu, S. C., and Zhu, T.:  
646 Photochemical production of ozone in Beijing during the 2008 Olympic Games,  
647 *Atmos. Chem. Phys.*, 11, 9825-9837, 10.5194/acp-11-9825-2011, 2011.
- 648 de Miranda, R. M., Andrade, M. D., and Fattori, A. P.: Preliminary studies of the effect  
649 of aerosols on nitrogen dioxide photolysis rates in the city of Sao Paulo, Brazil,  
650 *Atmospheric Research*, 75, 135-148, 10.1016/j.atmosres.2004.12.004, 2005.
- 651 Dickerson, R. R., Kondragunta, S., Stenchikov, G., Civerolo, K. L., Doddridge, B. G.,  
652 and Holben, B. N.: The Impact of Aerosols on Solar Ultraviolet Radiation and  
653 Photochemical Smog, *Science*, 278, 827-830, 10.1126/science.278.5339.827,  
654 1997.
- 655 Dubovik, O., and King, M. D.: A flexible inversion algorithm for retrieval of aerosol  
656 optical properties from Sun and sky radiance measurements, *Journal of*  
657 *Geophysical Research-Atmospheres*, 105, 20673-20696, 10.1029/2000jd900282,  
658 2000.
- 659 Fiore, A. M., Dentener, F. J., Wild, O., Cuvelier, C., Schultz, M. G., Hess, P., Textor, C.,  
660 Schulz, M., Doherty, R. M., Horowitz, L. W., MacKenzie, I. A., Sanderson, M. G.,  
661 Shindell, D. T., Stevenson, D. S., Szopa, S., Van Dingenen, R., Zeng, G., Atherton,  
662 C., Bergmann, D., Bey, I., Carmichael, G., Collins, W. J., Duncan, B. N., Faluvegi,  
663 G., Folberth, G., Gauss, M., Gong, S., Hauglustaine, D., Holloway, T., Isaksen, I.  
664 S. A., Jacob, D. J., Jonson, J. E., Kaminski, J. W., Keating, T. J., Lupu, A., Marmor,  
665 E., Montanaro, V., Park, R. J., Pitari, G., Pringle, K. J., Pyle, J. A., Schroeder, S.,



- 666 Vivanco, M. G., Wind, P., Wojcik, G., Wu, S., and Zuber, A.: Multimodel estimates  
667 of intercontinental source-receptor relationships for ozone pollution, *Journal of*  
668 *Geophysical Research-Atmospheres*, 114, 21, 10.1029/2008jd010816, 2009.
- 669 Fotiadi, A., Hatzianastassiou, N., Drakakis, E., Matsoukas, C., Pavlakis, K. G.,  
670 Hatzidimitriou, D., Gerasopoulos, E., Mihalopoulos, N., and Vardavas, I.: Aerosol  
671 physical and optical properties in the Eastern Mediterranean Basin, Crete, from  
672 Aerosol Robotic Network data, *Atmospheric Chemistry and Physics*, 6, 5399-5413,  
673 10.5194/acp-6-5399-2006, 2006.
- 674 Gao, W., Tie, X. X., Xu, J. M., Huang, R. J., Mao, X. Q., Zhou, G. Q., and Chang, L.  
675 Y.: Long-term trend of O<sub>3</sub> in a mega City (Shanghai), China: Characteristics,  
676 causes, and interactions with precursors, *Sci. Total Environ.*, 603, 425-433,  
677 10.1016/j.scitotenv.2017.06.099, 2017.
- 678 Gerasopoulos, E., Kazadzis, S., Vrekoussis, M., Kouvarakis, G., Liakakou, E.,  
679 Kouremeti, N., Giannadaki, D., Kanakidou, M., Bohn, B., and Mihalopoulos, N.:  
680 Factors affecting O<sub>3</sub> and NO<sub>2</sub> photolysis frequencies measured in the eastern  
681 Mediterranean during the five-year period 2002-2006, *Journal of Geophysical*  
682 *Research-Atmospheres*, 117, 14, 10.1029/2012jd017622, 2012.
- 683 Goliff, W. S., Stockwell, W. R., and Lawson, C. V.: The regional atmospheric chemistry  
684 mechanism, version 2, *Atmospheric Environment*, 68, 174-185,  
685 10.1016/j.atmosenv.2012.11.038, 2013.
- 686 Guo, S., Hu, M., Zamora, M. L., Peng, J., Shang, D., Zheng, J., Du, Z., Wu, Z., Shao,  
687 M., Zeng, L., Molina, M. J., and Zhang, R.: Elucidating severe urban haze  
688 formation in China, *Proceedings of the National Academy of Sciences*, 111,  
689 17373-17378, 10.1073/pnas.1419604111, 2014.
- 690 Han, T. T., Liu, X. G., Zhang, Y. H., Qu, Y., Gu, J. W., Ma, Q., Lu, K. D., Tian, H. Z.,  
691 Chen, J., Zeng, L. M., Hu, M., and Zhu, T.: Characteristics of Aerosol Optical  
692 Properties and Their Chemical Apportionments during CAREBeijing 2006,  
693 *Aerosol Air Qual. Res.*, 14, 1431-1442, 10.4209/aaqr.2013.06.0203, 2014.
- 694 Han, T. T., Liu, X. G., Zhang, Y. H., Qu, Y., Zeng, L. M., Hu, M., and Zhu, T.: Role of  
695 secondary aerosols in haze formation in summer in the Megacity Beijing, *Journal*  
696 *of Environmental Sciences*, 31, 51-60, 10.1016/j.jes.2014.08.026, 2015.
- 697 Han, T. T., Xu, W. Q., Li, J., Freedman, A., Zhao, J., Wang, Q. Q., Chen, C., Zhang, Y.  
698 J., Wang, Z. F., Fu, P. Q., Liu, X. G., and Sun, Y. L.: Aerosol optical properties  
699 measurements by a CAPS single scattering albedo monitor: Comparisons between  
700 summer and winter in Beijing, China, *Journal of Geophysical Research-*  
701 *Atmospheres*, 122, 2513-2526, 10.1002/2016jd025762, 2017.
- 702 Hendrick, F., Muller, J. F., Clemer, K., Wang, P., De Maziere, M., Fayt, C., Gielen, C.,  
703 Hermans, C., Ma, J. Z., Pinardi, G., Stavrakou, T., Vlemmix, T., and Van  
704 Roozendaal, M.: Four years of ground-based MAX-DOAS observations of HONO  
705 and NO<sub>2</sub> in the Beijing area, *Atmospheric Chemistry and Physics*, 14, 765-781,  
706 10.5194/acp-14-765-2014, 2014.
- 707 Hu, B., Zhao, X., Liu, H., Liu, Z., Song, T., Wang, Y., Tang, L., Xia, X., Tang, G., Ji,  
708 D., Wen, T., Wang, L., Sun, Y., and Xin, J.: Quantification of the impact of aerosol  
709 on broadband solar radiation in North China, *Scientific Reports*, 7, 44851,



- 710 10.1038/srep44851, 2017.
- 711 Jacobson, M. Z.: Studying the effects of aerosols on vertical photolysis rate coefficient  
712 and temperature profiles over an urban airshed, *Journal of Geophysical Research:*  
713 *Atmospheres*, 103, 10593-10604, 10.1029/98jd00287, 1998.
- 714 Jinfeng, Keding, Liuju, Zhong, Yubo, Duohong, Chen, Huang, Yuanhang, and Zhang:  
715 Fast increasing of surface ozone concentrations in Pearl River Delta characterized  
716 by a regional air quality monitoring network during 2006-2011, *Journal of*  
717 *Environmental Sciences*, 26, 23-36, 2014.
- 718 Lakey, P. S. J., George, I. J., Whalley, L. K., Baeza-Romero, M. T., and Heard, D. E.:  
719 Measurements of the HO<sub>2</sub> Uptake Coefficients onto Single Component Organic  
720 Aerosols, *Environ. Sci. Technol.*, 49, 4878-4885, 10.1021/acs.est.5b00948, 2015.
- 721 Lakey, P. S. J., George, I. J., Baeza-Romero, M. T., Whalley, L. K., and Heard, D. E.:  
722 Organics Substantially Reduce HO<sub>2</sub> Uptake onto Aerosols Containing Transition  
723 Metal ions, *Journal of Physical Chemistry A*, 120, 1421-1430,  
724 10.1021/acs.jpca.5b06316, 2016.
- 725 Lang, J. L., Zhang, Y. Y., Zhou, Y., Cheng, S. Y., Chen, D. S., Guo, X. U., Chen, S., Li,  
726 X. X., Xing, X. F., and Wang, H. Y.: Trends of PM<sub>2.5</sub> and Chemical Composition  
727 in Beijing, 2000-2015, *Aerosol Air Qual. Res.*, 17, 412-425,  
728 10.4209/aaqr.2016.07.0307, 2017.
- 729 Li, J., Chen, X. S., Wang, Z. F., Du, H. Y., Yang, W. Y., Sun, Y. L., Hu, B., Li, J. J.,  
730 Wang, W., Wang, T., Fu, P. Q., and Huang, H. L.: Radiative and heterogeneous  
731 chemical effects of aerosols on ozone and inorganic aerosols over East Asia, *Sci.*  
732 *Total Environ.*, 622, 1327-1342, 10.1016/j.scitotenv.2017.12.041, 2018.
- 733 Li, K., Jacob, D. J., Liao, H., Shen, L., Zhang, Q., and Bates, K. H.: Anthropogenic  
734 drivers of 2013-2017 trends in summer surface ozone in China, *Proceedings of the*  
735 *National Academy of Sciences of the United States of America*, 116, 422-427,  
736 10.1073/pnas.1812168116, 2019.
- 737 Liu, X., Zhang, Y., Jung, J., Gu, J., Li, Y., Guo, S., Chang, S.-Y., Yue, D., Lin, P., Kim,  
738 Y. J., Hu, M., Zeng, L., and Zhu, T.: Research on the hygroscopic properties of  
739 aerosols by measurement and modeling during CAREBeijing-2006, *Journal of*  
740 *Geophysical Research-Atmospheres*, 114, 10.1029/2008jd010805, 2009.
- 741 Liu, Z., Wang, Y., Gu, D., Zhao, C., Huey, L. G., Stickel, R., Liao, J., Shao, M., Zhu,  
742 T., Zeng, L., Amoroso, A., Costabile, F., Chang, C. C., and Liu, S. C.: Summertime  
743 photochemistry during CAREBeijing-2007: RO<sub>x</sub> budgets and O<sub>3</sub> formation,  
744 *Atmospheric Chemistry and Physics*, 12, 7737-7752, 10.5194/acp-12-7737-2012,  
745 2012.
- 746 Lou, S. J., Liao, H., and Zhu, B.: Impacts of aerosols on surface-layer ozone  
747 concentrations in China through heterogeneous reactions and changes in  
748 photolysis rates, *Atmospheric Environment*, 85, 123-138,  
749 10.1016/j.atmosenv.2013.12.004, 2014.
- 750 Lu, K., Fuchs, H., Hofzumahaus, A., Tan, Z., Wang, H., Zhang, L., Schmitt, S. H.,  
751 Rohrer, F., Bohn, B., Broch, S., Dong, H., Gkatzelis, G. I., Hohaus, T., Holland, F.,  
752 Li, X., Liu, Y., Liu, Y., Ma, X., Novelli, A., Schlag, P., Shao, M., Wu, Y., Wu, Z.,  
753 Zeng, L., Hu, M., Kiendler-Scharr, A., Wahner, A., and Zhang, Y.: Fast



- 754 Photochemistry in Wintertime Haze: Consequences for Pollution Mitigation  
755 Strategies, *Environ. Sci. Technol.*, 53, 10676-10684, 10.1021/acs.est.9b02422,  
756 2019.
- 757 Lu, K. D., Hofzumahaus, A., Holland, F., Bohn, B., Brauers, T., Fuchs, H., Hu, M.,  
758 Haseler, R., Kita, K., Kondo, Y., Li, X., Lou, S. R., Oebel, A., Shao, M., Zeng, L.  
759 M., Wahner, A., Zhu, T., Zhang, Y. H., and Rohrer, F.: Missing OH source in a  
760 suburban environment near Beijing: observed and modelled OH and HO<sub>2</sub>  
761 concentrations in summer 2006, *Atmospheric Chemistry and Physics*, 13, 1057-  
762 1080, 10.5194/acp-13-1057-2013, 2013.
- 763 Lu, X., Hong, J., Zhang, L., Cooper, O. R., Schultz, M. G., Xu, X., Wang, T., Gao, M.,  
764 Zhao, Y., and Zhang, Y.: Severe Surface Ozone Pollution in China: A Global  
765 Perspective, *Environmental Science & Technology Letters*, 5, 487-494,  
766 10.1021/acs.estlett.8b00366, 2018.
- 767 Ma, Z. Q., Xu, J., Quan, W. J., Zhang, Z. Y., Lin, W. L., and Xu, X. B.: Significant  
768 increase of surface ozone at a rural site, north of eastern China, *Atmospheric*  
769 *Chemistry and Physics*, 16, 3969-3977, 10.5194/acp-16-3969-2016, 2016a.
- 770 Ma, Z. W., Hu, X. F., Sayer, A. M., Levy, R., Zhang, Q., Xue, Y. G., Tong, S. L., Bi, J.,  
771 Huang, L., and Liu, Y.: Satellite-Based Spatiotemporal Trends in PM<sub>2.5</sub>  
772 Concentrations: China, 2004-2013, *Environmental Health Perspectives*, 124, 184-  
773 192, 10.1289/ehp.1409481, 2016b.
- 774 Madronich, S.: The Atmosphere and UV-B Radiation at Ground Level, in:  
775 *Environmental UV Photobiology*, edited by: Young, A. R., Moan, J., Björn, L. O.,  
776 and Nultsch, W., Springer US, Boston, MA, 1-39, 1993.
- 777 Matthews, P. S. J., Baeza-Romero, M. T., Whalley, L. K., and Heard, D. E.: Uptake of  
778 HO<sub>2</sub> radicals onto Arizona test dust particles using an aerosol flow  
779 tube, *Atmos. Chem. Phys.*, 14, 7397-7408, 10.5194/acp-14-7397-2014, 2014.
- 780 Mihelcic, D., Holland, F., Hofzumahaus, A., Hoppe, L., Konrad, S., Musgen, P., Patz,  
781 H. W., Schafer, H. J., Schmitz, T., Volz-Thomas, A., Bachmann, K., Schlomski, S.,  
782 Platt, U., Geyer, A., Alicke, B., and Moortgat, G. K.: Peroxy radicals during  
783 BERLIOZ at Pabstthum: Measurements, radical budgets and ozone production,  
784 *Journal of Geophysical Research-Atmospheres*, 108, 17, 10.1029/2001jd001014,  
785 2003.
- 786 Monks, P. S., Archibald, A. T., Colette, A., Cooper, O., Coyle, M., Derwent, R., Fowler,  
787 D., Granier, C., Law, K. S., Mills, G. E., Stevenson, D. S., Tarasova, O., Thouret,  
788 V., von Schneidmesser, E., Sommariva, R., Wild, O., and Williams, M. L.:  
789 Tropospheric ozone and its precursors from the urban to the global scale from air  
790 quality to short-lived climate forcer, *Atmospheric Chemistry and Physics*, 15,  
791 8889-8973, 10.5194/acp-15-8889-2015, 2015.
- 792 Ni, M. J., Huang, J. X., Lu, S. Y., Li, X. D., Yan, J. H., and Cen, K. F.: A review on  
793 black carbon emissions, worldwide and in China, *Chemosphere*, 107, 83-93,  
794 10.1016/j.chemosphere.2014.02.052, 2014.
- 795 Parrish, D. D., Xu, J., Croes, B., and Shao, M.: Air quality improvement in Los Angeles-  
796 perspectives for developing cities, *Frontiers of Environmental Science &*  
797 *Engineering*, 10, 10.1007/s11783-016-0859-5, 2016.



- 798 Peeters, J., Nguyen, T. L., and Vereecken, L.: HOx radical regeneration in the oxidation  
799 of isoprene, *Physical Chemistry Chemical Physics*, 11, 5935-5939,  
800 10.1039/b908511d, 2009.
- 801 Pollack, I. B., Ryerson, T. B., Trainer, M., Neuman, J. A., Roberts, J. M., and Parrish,  
802 D. D.: Trends in ozone, its precursors, and related secondary oxidation products in  
803 Los Angeles, California: A synthesis of measurements from 1960 to 2010, *Journal*  
804 *of Geophysical Research-Atmospheres*, 118, 5893-5911, 10.1002/jgrd.50472,  
805 2013.
- 806 Qu, W. J., Wang, J., Zhang, X. Y., Wang, D., and Sheng, L. F.: Influence of relative  
807 humidity on aerosol composition: Impacts on light extinction and visibility  
808 impairment at two sites in coastal area of China, *Atmospheric Research*, 153, 500-  
809 511, 10.1016/j.atmosres.2014.10.009, 2015.
- 810 Raga, G. B., Castro, T., and Baumgardner, D.: The impact of megacity pollution on  
811 local climate and implications for the regional environment: Mexico City,  
812 *Atmospheric Environment*, 35, 1805-1811, 10.1016/s1352-2310(00)00275-2,  
813 2001.
- 814 Real, E., and Sartelet, K.: Modeling of photolysis rates over Europe: impact on  
815 chemical gaseous species and aerosols, *Atmos. Chem. Phys.*, 11, 1711-1727,  
816 10.5194/acp-11-1711-2011, 2011.
- 817 Taketani, F., Kanaya, Y., and Akimoto, H.: Kinetics of heterogeneous reactions of HO<sub>2</sub>  
818 radical at ambient concentration levels with (NH<sub>4</sub>)<sub>2</sub>SO<sub>4</sub> and NaCl aerosol  
819 particles, *The Journal of Physical Chemistry A*, 112, 2370-2377, 2008.
- 820 Taketani, F., Kanaya, Y., Pochanart, P., Liu, Y., Li, J., Okuzawa, K., Kawamura, K.,  
821 Wang, Z., and Akimoto, H.: Measurement of overall uptake coefficients for HO<sub>2</sub>  
822 radicals by aerosol particles sampled from ambient air at Mts. Tai and Mang  
823 (China), *Atmospheric Chemistry and Physics*, 12, 11907-11916, 10.5194/acp-12-  
824 11907-2012, 2012.
- 825 Tan, Z., Fuchs, H., Lu, K., Hofzumahaus, A., Bohn, B., Broch, S., Dong, H., Gomm, S.,  
826 Häsel, R., He, L., Holland, F., Li, X., Liu, Y., Lu, S., Rohrer, F., Shao, M., Wang,  
827 B., Wang, M., Wu, Y., Zeng, L., Zhang, Y., Wahner, A., and Zhang, Y.: Radical  
828 chemistry at a rural site (Wangdu) in the North China Plain: observation and model  
829 calculations of OH, HO<sub>2</sub> and RO<sub>2</sub> radicals, *Atmos. Chem. Phys.*, 17, 663-690,  
830 10.5194/acp-17-663-2017, 2017.
- 831 Tian, R., Ma, X., Jia, H., Yu, F., Sha, T., and Zan, Y.: Aerosol radiative effects on  
832 tropospheric photochemistry with GEOS-Chem simulations, *Atmospheric*  
833 *Environment*, 208, 82-94, 2019.
- 834 Verstraeten, W. W., Neu, J. L., Williams, J. E., Bowman, K. W., Worden, J. R., and  
835 Boersma, K. F.: Rapid increases in tropospheric ozone production and export from  
836 China, *Nature geoscience*, 8, 690, 2015.
- 837 Wang, B., Shao, M., Lu, S. H., Yuan, B., Zhao, Y., Wang, M., Zhang, S. Q., and Wu, D.:  
838 Variation of ambient non-methane hydrocarbons in Beijing city in summer 2008,  
839 *Atmospheric Chemistry and Physics*, 10, 5911-5923, 10.5194/acp-10-5911-2010,  
840 2010.
- 841 Wang, J. L., Din, G. Z., and Chan, C. C.: Validation of a laboratory-constructed



- 842 automated gas chromatograph for the measurement of ozone precursors through  
843 comparison with a commercial analogy, *Journal of Chromatography A*, 1027, 11-  
844 18, 10.1016/j.chroma.2003.08.099, 2004.
- 845 Wang, M., Zeng, L., Lu, S., Shao, M., Liu, X., Yu, X., Chen, W., Yuan, B., Zhang, Q.,  
846 Hu, M., and Zhang, Z.: Development and validation of a cryogen-free automatic  
847 gas chromatograph system (GC-MS/FID) for online measurements of volatile  
848 organic compounds, *Analytical Methods*, 6, 9424-9434, 10.1039/c4ay01855a,  
849 2014.
- 850 Wang, M., Shao, M., Chen, W., Lu, S., Liu, Y., Yuan, B., Zhang, Q., Zhang, Q., Chang,  
851 C. C., Wang, B., Zeng, L., Hu, M., Yang, Y., and Li, Y.: Trends of non-methane  
852 hydrocarbons (NMHC) emissions in Beijing during 2002-2013, *Atmospheric  
853 Chemistry and Physics*, 15, 1489-1502, 10.5194/acp-15-1489-2015, 2015a.
- 854 Wang, Q. Q., Sun, Y. L., Jiang, Q., Du, W., Sun, C. Z., Fu, P. Q., and Wang, Z. F.:  
855 Chemical composition of aerosol particles and light extinction apportionment  
856 before and during the heating season in Beijing, China, *Journal of Geophysical  
857 Research-Atmospheres*, 120, 12708-12722, 10.1002/2015jd023871, 2015b.
- 858 Wang, W., Li, X., Shao, M., Hu, M., Zeng, L., Wu, Y., and Tan, T.: The impact of  
859 aerosols on photolysis frequencies and ozone production in Beijing during the 4-  
860 year period 2012–2015, *Atmos. Chem. Phys.*, 19, 9413-9429, 10.5194/acp-19-  
861 9413-2019, 2019.
- 862 Wang, X. M., Chen, W. H., Chen, D. H., Wu, Z. Y., and Fan, Q.: Long-term trends of  
863 fine particulate matter and chemical composition in the Pearl River Delta  
864 Economic Zone (PRDEZ), China, *Frontiers of Environmental Science &  
865 Engineering*, 10, 53-62, 10.1007/s11783-014-0728-z, 2016.
- 866 Wang, Y., Zhang, Y., Hao, J., and Luo, M.: Seasonal and spatial variability of surface  
867 ozone over China: contributions from background and domestic pollution,  
868 *Atmospheric Chemistry and Physics*, 11, 3511-3525, 10.5194/acp-11-3511-2011,  
869 2011.
- 870 Warneke, C., de Gouw, J. A., Holloway, J. S., Peischl, J., Ryerson, T. B., Atlas, E., Blake,  
871 D., Trainer, M., and Parrish, D. D.: Multiyear trends in volatile organic compounds  
872 in Los Angeles, California: Five decades of decreasing emissions, *Journal of  
873 Geophysical Research-Atmospheres*, 117, 10.1029/2012jd017899, 2012.
- 874 Wehner, B., Birmili, W., Ditas, F., Wu, Z., Hu, M., Liu, X., Mao, J., Sugimoto, N., and  
875 Wiedensohler, A.: Relationships between submicrometer particulate air pollution  
876 and air mass history in Beijing, China, 2004-2006, *Atmospheric Chemistry and  
877 Physics*, 8, 6155-6168, 10.5194/acp-8-6155-2008, 2008.
- 878 Wendisch, M., Mertes, S., Ruggaber, A., and Nakajima, T.: Vertical profiles of aerosol  
879 and radiation and the influence of a temperature inversion: Measurements and  
880 radiative transfer calculations, *J. Appl. Meteorol.*, 35, 1703-1715, 10.1175/1520-  
881 0450(1996)035<1703:vpoaar>2.0.co;2, 1996.
- 882 Xie, X., Shao, M., Liu, Y., Lu, S., Chang, C.-C., and Chen, Z.-M.: Estimate of initial  
883 isoprene contribution to ozone formation potential in Beijing, China, *Atmospheric  
884 Environment*, 42, 6000-6010, 10.1016/j.atmosenv.2008.03.035, 2008.
- 885 Xu, J., Ma, J. Z., Zhang, X. L., Xu, X. B., Xu, X. F., Lin, W. L., Wang, Y., Meng, W.,



- 886 and Ma, Z. Q.: Measurements of ozone and its precursors in Beijing during  
887 summertime: impact of urban plumes on ozone pollution in downwind rural areas,  
888 Atmospheric Chemistry and Physics, 11, 12241-12252, 10.5194/acp-11-12241-  
889 2011, 2011.
- 890 Xu, J., Zhang, Y. H., Zheng, S. Q., and He, Y. J.: Aerosol effects on ozone  
891 concentrations in Beijing: A model sensitivity study, J. Environ. Sci., 24, 645-656,  
892 10.1016/s1001-0742(11)60811-5, 2012.
- 893 Yuan, B., Shao, M., de Gouw, J., Parrish, D. D., Lu, S., Wang, M., Zeng, L., Zhang, Q.,  
894 Song, Y., Zhang, J., and Hu, M.: Volatile organic compounds (VOCs) in urban air:  
895 How chemistry affects the interpretation of positive matrix factorization (PMF)  
896 analysis, Journal of Geophysical Research-Atmospheres, 117,  
897 10.1029/2012jd018236, 2012.
- 898 Zhang, J. P., Zhu, T., Zhang, Q. H., Li, C. C., Shu, H. L., Ying, Y., Dai, Z. P., Wang, X.,  
899 Liu, X. Y., Liang, A. M., Shen, H. X., and Yi, B. Q.: The impact of circulation  
900 patterns on regional transport pathways and air quality over Beijing and its  
901 surroundings, Atmospheric Chemistry and Physics, 12, 5031-5053, 10.5194/acp-  
902 12-5031-2012, 2012.
- 903 Zhang, L., Shao, J. Y., Lu, X., Zhao, Y. H., Hu, Y. Y., Henze, D. K., Liao, H., Gong, S.  
904 L., and Zhang, Q.: Sources and Processes Affecting Fine Particulate Matter  
905 Pollution over North China: An Adjoint Analysis of the Beijing APEC Period,  
906 Environ. Sci. Technol., 50, 8731-8740, 10.1021/acs.est.6b03010, 2016.
- 907 Zhang, Q., Yuan, B., Shao, M., Wang, X., Lu, S., Lu, K., Wang, M., Chen, L., Chang,  
908 C. C., and Liu, S. C.: Variations of ground-level O<sub>3</sub> and its precursors in Beijing  
909 in summertime between 2005 and 2011, Atmospheric Chemistry and Physics, 14,  
910 6089-6101, 10.5194/acp-14-6089-2014, 2014.
- 911 Zhao, B., Wang, S. X., Liu, H., Xu, J. Y., Fu, K., Klimont, Z., Hao, J. M., He, K. B.,  
912 Cofala, J., and Amann, M.: NO<sub>x</sub> emissions in China: historical trends and future  
913 perspectives, Atmospheric Chemistry and Physics, 13, 9869-9897, 10.5194/acp-  
914 13-9869-2013, 2013.
- 915 Zhao, P. S., Zhang, X. L., and Xu, X. F.: Long-term visibility trends and characteristics  
916 in the region of Beijing, Tianjin, and Hebei, China, Abstr. Pap. Am. Chem. Soc.,  
917 242, 1, 2011.
- 918 Zheng, C., Zhao, C., Zhu, Y., Wang, Y., Shi, X., Wu, X., Chen, T., Wu, F., and Qiu, Y.:  
919 Analysis of influential factors for the relationship between PM<sub>2.5</sub> and AOD in  
920 Beijing, Atmospheric Chemistry and Physics, 17, 13473-13489, 2017.
- 921 Zou, Q., Song, H., Tang, M., and Lu, K.: Measurements of HO<sub>2</sub> uptake coefficient on  
922 aqueous (NH<sub>4</sub>)<sub>2</sub>SO<sub>4</sub> aerosol using aerosol flow tube with LIF system, Chinese  
923 Chemical Letters, 30, 2236-2240, <https://doi.org/10.1016/j.ccl.2019.07.041>,  
924 2019.
- 925